POLITECNICO DI TORINO
Repository ISTITUZIONALE

Nanoremediation of Contaminated Aquifers: Injection Modeling for Field-Scale Design

Original
Nanoremediation of Contaminated Aquifers: Injection Modeling for Field-Scale Design / Mondino, Federico; Bianco, Carlo; Tosco, Tiziana; Casasso, Alessandro; Sethi, Rajandrea. - In: WATER. - ISSN 2073-4441. - ELETTRONICO. - 18:6(2026), pp. 1-12. [10.3390/w18060700]

Availability:
This version is available at: 11583/3009087 since: 2026-03-24T08:03:06Z

Publisher:
MDPI

Published
DOI:10.3390/w18060700

Terms of use:

This article is made available under terms and conditions as specified in the corresponding bibliographic description in the repository

Publisher copyright

(Article begins on next page)

31 May 2026

water

MDPI

Article

Nanoremediation of Contaminated Aquifers: Injection Modeling for Field-Scale Design

Federico Mondino, Carlo Bianco, Tiziana Tosco, Alessandro Casasso * and Rajandrea Sethi

Department of Environment, Land and Infrastructure Engineering (DIATI), Politecnico di Torino, Corso Duca degli Abruzzi 24, 10129 Torino, Italy; federico.mondino@polito.it (F.M.); carlo.bianco@polito.it (C.B.); tiziana.tosco@polito.it (T.T.); rajandrea.sethi@polito.it (R.S.)

* Correspondence: alessandro.casasso@polito.it; Tel.: +39-0110907622

Abstract

The subsurface injection of nanoparticles dispersed in stabilizing suspensions has emerged in the last 20 years as an effective and efficient remediation technique. The stabilizing suspensions used to avoid particle aggregation are shear-thinning—and hence non-Newtonian—fluids. In addition, the relatively high groundwater velocities and the high fluid viscosity do not allow for the application of the Darcy's law, which must be replaced with the Forchheimer's law. For these reasons, the calculation of the pressure drop in porous media has so far been performed numerically. In this article, a novel analytical formula is derived through a series of simplifying assumptions, using the Cross–Carreau formulation to describe the shear-thinning rheological behavior of the injected fluid. The validity of the formula was assessed using the numerical model MNMs. Comparison between the analytical predictions and the numerical results showed good agreement, with a substantial overlap of the results. For these reasons, the explicit formula is considered a useful tool to support the field-scale design of injection interventions.

Keywords: shear-thinning fluid; non-Newtonian fluid; porous media; nanoremediation; zero-valent iron

1. Introduction

Among applications in environmental clean-up technologies, nanoremediation has gradually emerged as a competitive, state-of-the-art technology for generating reactive zones in the aquifer [1–3]. This approach consists of injecting aqueous suspensions of reactive micro- and nanoparticles into the aquifer to induce the degradation, transformation and/or in situ immobilization of pollutants [4–6]. Among the nanomaterials studied or applied in the field of nanoremediation, zero-valent iron-based materials are of the greatest interest for the treatment of contamination by halogenated organic compounds, heavy metals, and DDT [7–13].

A key aspect in the application of nanoremediation is the effective control of the particle injection phase and, in order to improve and optimize the groundwater distribution of nanoreagents, natural polymeric solutions are often used. In particular, zero-valent iron particles are generally stabilized with carboxymethylcellulose, guar gum, or xanthan gum [14,15]. These polymers modify the surface properties of the particles (limiting their aggregation) and the viscosity of the dispersing fluid, and are characterized by a shear-thinning behavior, which provides high viscosity in static conditions, thus limiting particles' aggregation and sedimentation, and lower viscosity in dynamic conditions, thus

Check for updates

Academic Editors: Chin H Wu and Zbigniew Kabala

Received: 14 October 2025
Revised: 23 February 2026
Accepted: 7 March 2026
Published: 17 March 2026

Copyright: © 2026 by the authors. Licensee MDPI, Basel, Switzerland. This article is an open access article distributed under the terms and conditions of the Creative Commons Attribution (CC BY) license.

helping to limit the pressure increase during injection [16,17]. Moreover, it has been proved experimentally that shear-thinning fluids exhibit enhanced dispersion in porous media, in contrast to Newtonian fluids where dispersivity is constant and controlled solely by the porous medium's properties [18]. This characteristic could contribute to a more distributed delivery of the particles in proximity to injection points.

When non-Newtonian fluids are considered, good knowledge of their rheological properties is required to extend Darcy's law to flow regimes involving fluids with variable viscosity. To this purpose, several authors proposed different rheological models to describe non-Newtonian fluids, such as Ellis [19], Cross [20], Carreau [21] and Ostwald de Waele [22]. In a wide range of applications that involve non-Newtonian fluids, such as the above-mentioned one in environmental engineering, it is of pivotal importance to assess the pressure drop induced by a non-Newtonian fluid flowing through a porous medium. Darcy's law [23] is the most used linear equation for describing single-phase steady-state Newtonian fluid flow through a saturated porous medium. However, in aquifer systems as well as in oil and gas reservoirs, non-linear flow can occur in the proximity of the pumping (or injecting) well due to the high fluid velocities reached. Hassanizadeh and Gray (1987) [24] demonstrated that, starting from Reynolds numbers in the order of 10, this non-linearity arises due to microscale drag forces. Levy et al. (1999) [25] attributed the non-linearities to inertial effects, whereas Dybbs and Edwards (1984) [26] identified the cause in low Reynolds number turbulence at the solid–liquid interface. Forchheimer (1901) [27] first proposed the currently most widely used expression to describe these non-linearities, adding a quadratic term to Darcy's law.

Several authors [28] have emphasized the utility of simple analytical models for preliminary assessments in the management of contaminated sites, and as a support in the first steps of remediation design, as they offer a conservative, rapid, and cost-effective approach. Such models are expected to be straightforward to apply, and to enable efficient estimations, thus being particularly valuable for field-scale design and planning in the absence of detailed site-specific data, or when complex numerical simulations are not yet feasible.

With similar purposes, this study derives an equation able to describe the spatial distribution of the increment of pressure generated by the injection of a non-Newtonian shear-thinning fluid in a porous medium as a function of both time and radial distance from the injection well. The equation is based on the Forchheimer modification of Darcy's law, summarized in Section 2.1, and on the rheological model of Cross for shear-thinning fluids, presented in Section 2.2. The use of the pressure increase equation developed here is presented in Section 2.3, and its use is demonstrated in Section 3 with a validation against numerical modeling results with the software MNMs (https://areeweb.polito.it/ricerca/groundwater/software/mnms/ (accessed on 12 December 2025)), previously developed and validated by the authors, in a synthetic case, performing several sensitivity analyses on the main operative parameters (polymer concentration and flow rate) and aquifer properties (permeability) that influence the rise in pressure during the injection.

2. Governing Equations

2.1. Darcy–Forchheimer Equation

Darcy's law defines a linear relationship between the pressure drop and flow rate through a porous medium [23]. However, when fluid velocities are very high, such as near to a wellbore during injection, this assumption is not met anymore. Forchheimer (1901) [27] therefore suggested modifying the Darcy law by adding an empirical non-linear quadratic term:

$$\frac{\partial p}{\partial x} = \frac{\mu}{K_0} q + \beta \rho q^2 \quad (1)$$

where p is the pressure of the fluid [$ML^{-1}T^{-2}$]; q is the specific discharge of the fluid, also known as the Darcy velocity [LT^{-1}]; K_0 is the porous medium's intrinsic permeability [L^2]; μ is the fluid viscosity [$ML^{-1}T^{-1}$]; ρ is the fluid density [ML^{-3}]; and β [L^{-1}] is the so-called inertial flow coefficient.

Several authors have proposed theoretical and empirical correlations for the inertial flow coefficient β, which are primarily expressed as functions of intrinsic permeability, porosity, and tortuosity [29–31]. The inertial flow coefficient is therefore an intrinsic property of the porous medium, being dependent on permeability and independent of the fluid properties.

The quadratic term in the Darcy–Forchheimer equation is more relevant for high Darcy velocities and for small porosity and permeability values, but it is independent of the fluid viscosity [32].

2.2. Cross Rheological Model

During the injection of a non-Newtonian shear-thinning fluid in a porous medium, the apparent viscosity of the polymeric fluid is a function of the shear rate $\dot{\gamma}$ [T^{-1}]. In particular, it is constant at very high and very low shear rates, and decreases with increasing shear rates in an intermediate region. This behavior can be modeled with the Cross–Carreau formulation [20,21]:

$$\mu_p(\dot{\gamma}) = \mu_\infty + \frac{\mu_0 - \mu_\infty}{1 + (\lambda\dot{\gamma})^\chi} \tag{2}$$

where μ_0 is the zero-shear rate viscosity [$ML^{-1}T^{-1}$]; μ_∞ is the limiting viscosity [$ML^{-1}T^{-1}$] for $\dot{\gamma} \to \infty$; λ [T] is the time constant, i.e., the reciprocal of the shear rate which separates the first Newtonian plateau from the power-law region; and χ is the model exponent [-].

Recalling that in a radial flow field the Darcy velocity q is not constant, but it declines hyperbolically with the distance r from an injection point, following $q = Q/(2\pi rb)$ [33], and that the shear rate experienced by a fluid flowing through a porous medium, called apparent shear rate $\dot{\gamma}_m$, is inversely proportional to the square root of permeability and porosity [34], it is possible to express the apparent shear rate as:

$$\dot{\gamma}_m = \alpha\frac{Q}{2\pi rb\sqrt{K_0\varepsilon}} \tag{3}$$

where Q is the discharge rate [L^3T^{-1}], b is the vertical length of the well screen [L], r is the radial distance from the injection point, ε is the effective porosity, and α is the shift factor [-] introduced to superimpose rheograms obtained from rotational tests and those corresponding to the flow through the porous medium [35].

Substituting Equation (3) in Equation (2) it is possible to obtain an expression of viscosity as a function of the radial distance:

$$\mu_p(r) = \mu_\infty + \frac{\mu_0 - \mu_\infty}{1 + \left(\frac{\lambda\alpha Q}{2\pi br\sqrt{K_0\varepsilon}}\right)^\chi} \tag{4}$$

2.3. Quasi-Steady-State Flow Equation

The total pressure drop induced by the injection of a non-Newtonian shear-thinning fluid towards a fully penetrating well located in a confined, homogenous and isotropic aquifer with homogeneous thickness can be calculated in a radial domain, unlimited on the horizontal plane, as the sum of four contributions:

$$\Delta p_{tot} = \Delta p_p\Big]_{r_w}^{r_a} + \Delta p_{p\beta}\Big]_{r_w}^{r_a} + \Delta p_w\Big]_{r_a}^{R} + \Delta p_{w\beta}\Big]_{r_a}^{R} \tag{5}$$

where subscripts p and w in the pressure drop terms Δp refer respectively to the non-Newtonian shear-thinning fluid (in the case of nanoparticle suspensions, the polymeric solution in which particles are dispersed) and to the water, while the subscript β denotes the pressure drop term associated with the quadratic term in the Darcy–Forchheimer flow's law (see Equation (1)). Radial symmetry is assumed under the hypothesis that the radial flow generated by the injection through the wells dominates over the natural background flow. The total pressure drop in Equation (5) is split into four contributions, respectively linear and non-linear pressure drops from the well radius r_w to the theoretical radius of influence for the polymeric solution r_a (first and second terms), and linear and non-linear pressure drops from r_a to the radius of influence of water R, i.e., the distance at which the hydraulic head remains at its initial value [36] (third and fourth terms).

Each term in Equation (5) is a function of both time and distance. The theoretical radius of influence for the polymeric solution r_a at any time t can be calculated as

$$r_a = \sqrt{\frac{Qt}{\pi b \varepsilon}} \tag{6}$$

The first term in Equation (5) describes the pressure drop Δp_p induced by the polymeric solution injection due to viscous resistance in steady-state conditions. This, accordingly with Thiem (1906) [37], gives:

$$\Delta p_p \Big]_{r_w}^{r_a} = \frac{Q}{2\pi b K_0} \left(\mu_\infty ln \frac{r_a}{r_w} + \frac{(\mu_0 - \mu_\infty)}{\chi} \ln \left(\frac{\left(\frac{\lambda \alpha Q}{2\pi b \sqrt{K_0 \varepsilon}} \right)^\chi + r_a^\chi}{\left(\frac{\lambda \alpha Q}{2\pi b \sqrt{K_0 \varepsilon}} \right)^\chi + r_w^\chi} \right) \right) \tag{7}$$

Appendix A shows the detailed integration leading to Equation (7).

The third term in Equation (5) describes the pressure drop due to water flow in the transient state, from the theoretical radius of influence for the polymeric solution r_a up to the radius of influence R [L], as described by Cooper and Jacob [38]:

$$\Delta p_w \Big]_{r_a}^{R} \approx \frac{Q \mu_w}{4\pi b K_0} ln \left(2.25 \frac{b \rho_w g K_0 t}{\mu_w S_s r_a^2} \right) \tag{8}$$

where μ_w is water viscosity [$ML^{-1}T^{-1}$], ρ_w is water density [ML^{-3}], g is gravitational acceleration [LT^{-2}], S is the aquifer storativity [-], and t is time [T]. Equation (8) is valid for times such that $t \geq 12.5\ \mu_w S_s r_a^2 / \rho g K_0$.

Finally, the second and fourth terms in Equation (5) describe the non-linear pressure drops due to both polymeric solution and water flow. These values are calculated by integrating the non-linear term of Equation (1) from the well radius r_w up to the radius of influence of the polymeric solution r_a and from there to the distance R at which the hydraulic head remains at its initial value. The non-linear contribution of both the polymeric solution (9) and water (10) are given respectively by:

$$\Delta p_{p\beta} \Big]_{r_w}^{r_a} = \int_{r_w}^{r_a} \beta \rho_p q^2 dr = \beta \rho_p \left(\frac{Q}{2\pi b} \right)^2 \left(\frac{1}{r_w} - \frac{1}{r_a} \right) \tag{9}$$

$$\Delta p_{w\beta} \Big]_{r_a}^{R} = \int_{r_a}^{R} \beta \rho_w q^2 dr = \beta \rho_w \left(\frac{Q}{2\pi b} \right)^2 \left(\frac{1}{r_a} - \frac{1}{R} \right) \tag{10}$$

where, as stated for Equation (3), the Darcy velocity q in a radial flow field decreases hyperbolically with distance r.

Since polymer concentrations in the order of a few g/L are usually sufficient to improve the colloidal stability of remediation slurries [14], and for such a low concentration

it is fairly acceptable to assume no significant change in fluid density due to the presence of the dissolved polymer, $\rho_p \approx \rho_w$, Equations (9) and (10) can be combined to calculate the overall non-linear pressure increase:

$$\Delta p_{p\beta}\Big]_{r_w}^{r_a} + \Delta p_{w\beta}\Big]_{r_a}^{R} = \int_{r_w}^{R} \beta\rho_w q^2 dr = \beta\rho_w \left(\frac{Q}{2\pi b}\right)^2 \left(\frac{1}{r_w} - \frac{1}{R}\right) \tag{11}$$

Since R is orders of magnitude larger than r_w, its reciprocal can be neglected.

In conclusion, Equation (5) can be re-written as:

$$\Delta p_{tot} = \frac{Q\mu_w}{4\pi K_0 b}\int_u^{\infty} \frac{e^{-u}}{u} du + \frac{Q(\mu_\infty - \mu_w)}{2\pi K_0 b}\left(ln\frac{r_a}{r_w} + \frac{\mu_0 - \mu_\infty}{\chi\,(\mu_\infty - \mu_w)}\ln\left(\frac{\left(\frac{\lambda\alpha Q}{2\pi b\sqrt{K_0\varepsilon}}\right)^{\chi} + r_a^{\chi}}{\left(\frac{\lambda\alpha Q}{2\pi b\sqrt{K_0\varepsilon}}\right)^{\chi} + r_w^{\chi}}\right)\right) + \left(\frac{Q}{2\pi b}\right)^2 \frac{\beta\rho_w}{r_w} \tag{12}$$

where $u = S_s r_w^2 \mu_w / 4\rho_w g K_0 t$ as defined by Theis [39]. Appendix B shows the detailed derivation of Equation (12). It is worth noting that the first term in (12) is the Theis solution for the transient state evaluated in the well. Since the water pressure drop has already been taken into account in the overlapping range between r_w and r_a, the second term only describes the polymeric solution contribution in a steady state.

3. Application to a Synthetic Case

Equation (12) was tested to simulate the injection through a vertical fully penetrating well of a non-Newtonian shear-thinning fluid in a confined, homogenous and isotropic aquifer with even thickness unlimited on the horizontal plane. This aquifer is characterized by a permeability $K_0 = 5.0 \times 10^{-11}$ m^2, a specific storage $S_S = 2.0 \times 10^4$ m^{-1}, a porosity $\varepsilon = 0.2$ and an inertial flow coefficient $\beta = 7.0 \times 10^4$ m^{-1}, values typical of a sandy aquifer. The well has a radius $r_w = 0.02$ m and the ratio between the discharge rate and vertical length of the well screen is $Q/b = 1$ m^3/h/m. The rheological parameters were derived from Gastone et al. (2014) [14] and, for a 3 g/L guar gum solution (GG), they are: $\mu_0 = 1.56 \times 10^{-1}$ Pa·s, $\mu_\infty = 3.47 \times 10^{-3}$ Pa·s, $\lambda = 4.28 \times 10^{-2}$ s and $\chi = 0.713$ [14]. For simplicity, a shift factor $\alpha = 1$ has been assumed. Temperature-induced viscosity variations are considered negligible under typical aquifer injection conditions, while processes such as polymer adsorption and retention onto the aquifer material—potentially relevant depending on the slurry preparation, polymer type and porous matrix superficial properties—are beyond the scope of the present analytical formulation and would require numerical modeling approaches.

Figure 1 shows the temporal evolution of the total pressure increase in the injection well computed using the above parameters for different guar gum concentrations, and its comparison with the results obtained from simulations performed with the MNMs numerical model [40]. The full set of equations solved in MNMs is reported in the Supporting Information. The MNMs model has been shown to reliably predict transport properties even under complex experimental conditions, as demonstrated in the Supporting Information and in Mondino et al. [41]. Figure 2 shows the pressure drop in the same conditions but as a function of distance from the well; different curves at different fixed times represent the evolution of the injection. Again, the analytical model proposed in this paper is validated against the results of the numerical software MNMs v.3.019. This use of Equation (12) could be useful, for example, to avoid a "short circuit" between the injection well and other wells/piezometers at close distances. Figure 3 shows the radial distributions of the pressure drop for different GG concentrations, after 1 h from the beginning of the injection

at a 1 $m^3/h/m$ flow rate, and Figure 4 shows the modest impact of the well radius on the injection process.

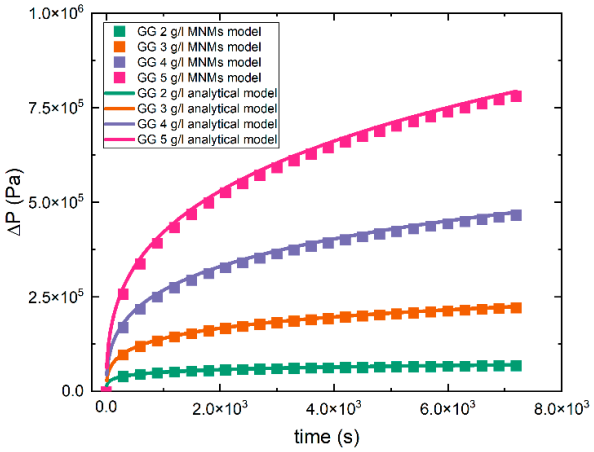

Figure 1. Time series of the pressure drop for the injection of a guar gum solution at different concentrations (coefficient of determination between analytical solution and MNMs simulation: GG 2 g/L, R^2 = 0.953, GG 3 g/L, R^2 = 0.992, GG 4 g/L, R^2 = 0.990, and GG 5 g/L, R^2 = 0.992).

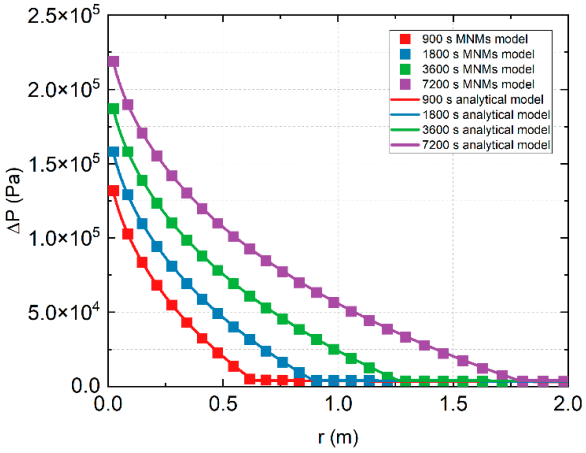

Figure 2. Radial distribution of the pressure drop for the injection of a guar gum solution at 3 g/L, at different times (coefficient of determination between analytical solution and MNMs simulation: 900 s, R^2 = 0.999, 1800 s, R^2 = 0.999, 3600 s, R^2 = 0.999, and 7200 s, R^2 = 0.999).

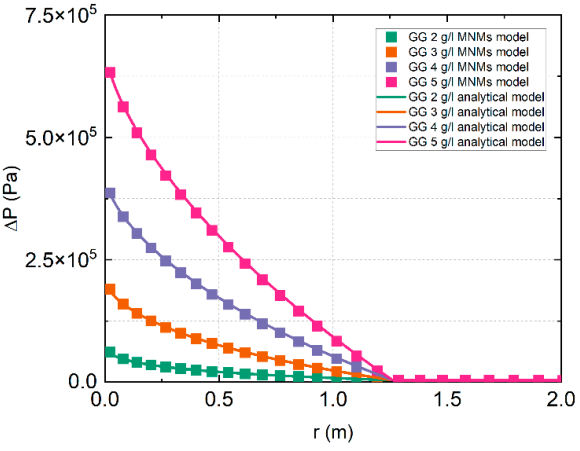

Figure 3. Radial distributions of the pressure drop after 1 h of injection, for different values of the GG concentration (coefficient of determination between analytical solution and MNMs simulation: GG 2 g/L, R^2 = 0.999, GG 3 g/L, R^2 = 0.999, GG 4 g/L, R^2 = 0.999 and GG 5 g/L, R^2 = 0.999).

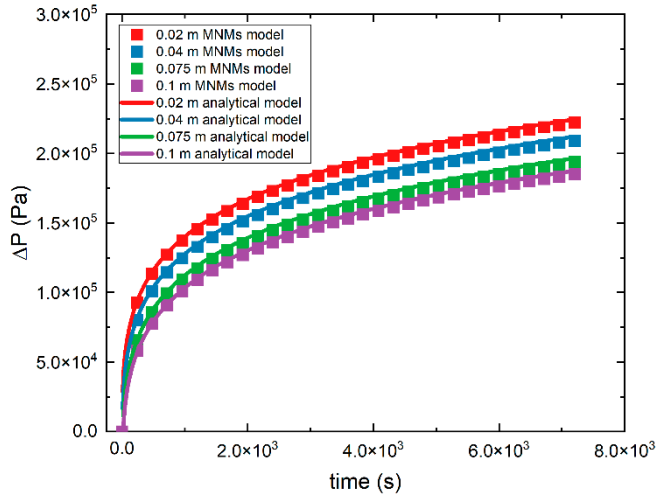

Figure 4. Time series of the total pressure drop for the injection of a 3 g/L GG solution with different well radii (0.02–1 m) (coefficient of determination between analytical solution and MNMs simulation: 0.02 m, R^2 = 0.997, 0.04 m, R^2 = 0.995, 0.075 m, R^2 = 0.996 and 0.1 m, R^2 = 0.996).

Finally, Figure 5 highlights the substantial impact associated with variations in the permeability of the porous medium over a range of two orders of magnitude.

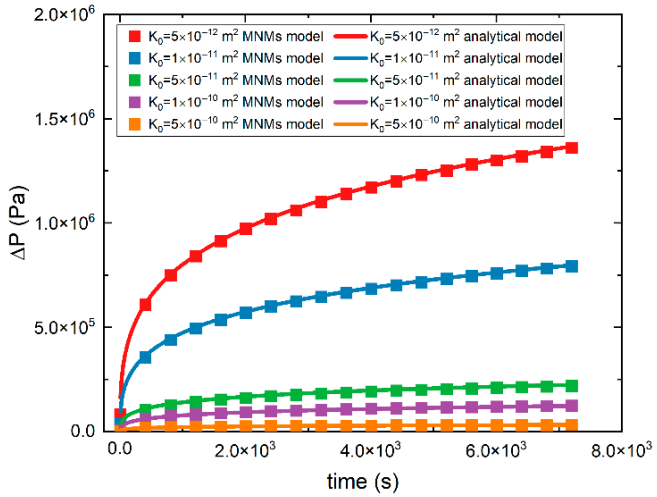

Figure 5. Time series of the total pressure drop for the injection of a 3 g/L GG solution in aquifers with different permeabilities (coefficient of determination between analytical solution and MNMs simulation: 5×10^{-12} m^2, R^2 = 0.999, 1×10^{-11} m^2, R^2 = 0.998, 5×10^{-11} m^2, R^2 = 0.970, 1×10^{-10} m^2, R^2 = 0.998 and 5×10^{-10} m^2, R^2 = 0.985).

The two approaches—i.e., the analytical formula herein proposed and the software MNMs—describe the same physical problem using fundamentally different methodologies, namely, a polymer advection–dispersion equation in MNMs versus a combination of steady-state and transient analytical formulations in the analytical formula. This systematic agreement provides a robust and independent validation of the analytical model.

Compared with classical formulations, such as that of Cooper and Jacob, Equation (12) accounts for non-Newtonian fluids and integrates the expected behavior under both transient and steady-state conditions, thereby enabling its use as a practical tool for injection sizing. Indeed, it is possible to calculate the maximum pressure reached in the well during the injection of a chosen volume of polymeric solution as a function of the discharge rate, based on the well geometry, the rheological properties of the fluid and the fracturing pressure of the porous media. Figure 6 shows, for example, the effect of setting a fracturing

pressure threshold of 2.5 bar to inject different volumes of suspension (from 0.5 m^3/m to 2 m^3/m). While a maximum flow rate of about 1 $m^3/h/m$ can be used to inject 2 m^3/m, the flow rate increases to about 2.2 $m^3/h/m$ if only 0.5 m^3/m is injected.

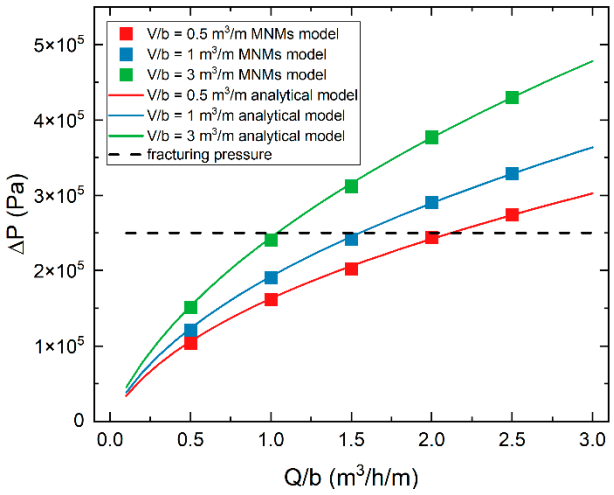

Figure 6. Maximum pressure increase ΔP against the normalized discharge rate Q/b injecting GG at 3 g/L through a well (r_w = 0.02 m) at different slurry volumes injected per unit thickness of aquifer V/b (coefficient of determination between analytical solution and MNMs simulation: 0.5 m^3/m, R^2 = 0.999, 1.0 m^3/m, R^2 = 0.999 and 2.0 m^3/m, R^2 = 0.999).

Since the polymeric solution concentration could also be a variable during the dimensioning phase, in Figure 7 the planes representing the maximum pressure reached for different guar gum concentrations are represented as a function of both time and the normalized discharge rate.

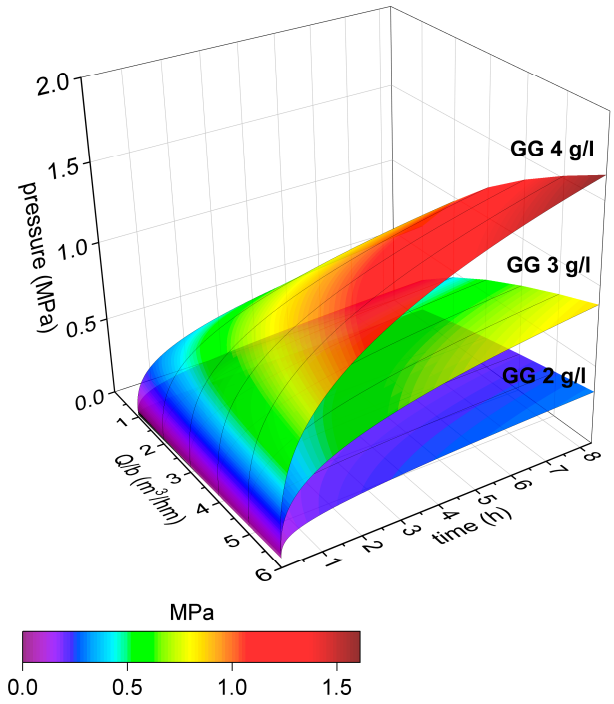

Figure 7. Isosurface of the maximum pressure reached for the injection of 1 m^3 of guar gum solution through a well (r_w = 0.02 m) as a function of both normalized discharge rate and concentration of polymeric solution.

4. Conclusions

The injection of nanoparticles for the remediation of contaminated aquifers requires a thorough understanding of the propagation of high-viscosity, shear-thinning fluids in which such particles are suspended, in order to prevent aggregation phenomena.

In this paper, an explicit analytical formula was derived to calculate the radial distribution of the pressure drop around an injection well. The formulation is based on the Forchheimer extension of Darcy's law and employs the Cross–Carreau model to reproduce the shear-thinning behavior of polymer suspensions. To the authors' knowledge, no analytical solution was previously available for this problem, which was typically solved numerically with the support of dedicated software.

The ability to predict the pressure drop through an explicit analytical expression enables the rapid design and preliminary assessment of nanoremediation interventions, such as estimating maximum injection flow rates that avoid fracturing of the porous medium, evaluating the effects of changes in the polymer type and concentration or well radius, and performing sensitivity analyses on uncertain parameters. The accuracy of the proposed formulation was quantitatively assessed through comparison with numerical simulations. The results show a strong agreement between analytical and numerical predictions within the range of conditions investigated, supporting the reliability of Equation (12) for its intended application.

Supplementary Materials: The following supporting information can be downloaded at: https://www.mdpi.com/article/10.3390/w18060700/s1.

Author Contributions: Conceptualization, C.B., F.M., A.C., R.S.; methodology, C.B., F.M., R.S.; software, C.B., F.M.; writing—original draft preparation, C.B., F.M., A.C.; writing—review and editing, A.C., C.B., T.T., R.S.; supervision, R.S.; funding acquisition, R.S. All authors have read and agreed to the published version of the manuscript.

Funding: This research received no external funding.

Data Availability Statement: The original contributions presented in this study are included in the article and Supplementary Material. Further inquiries can be directed to the corresponding author.

Conflicts of Interest: The authors declare no conflicts of interest.

Appendix A

The pressure drop Δp_p induced by the polymeric solution injection due to viscous resistance in steady-state conditions, according to Thiem (1906) [37], is given by:

$$\Delta p_p = \frac{Q}{2\pi b K_0}\int_{r_w}^{r_a} \mu_p(r)\frac{1}{r}dr = \frac{Q}{2\pi b K_0}\int_{r_w}^{r_a}\left(\mu_\infty + \frac{\mu_0-\mu_\infty}{1+\left(\frac{\lambda\alpha Q}{2\pi b r\sqrt{K_0\varepsilon}}\right)^{\chi}}\right)\frac{1}{r}dr$$
$$= \frac{Q}{2\pi b K_0}\left(\mu_\infty\int_{r_w}^{r_a}\frac{1}{r}dr + (\mu_0-\mu_\infty)\int_{r_w}^{r_a}\frac{1}{1+\left(\frac{\lambda\alpha Q}{2\pi b r\sqrt{K_0\varepsilon}}\right)^{\chi}}\frac{1}{r}dr\right)$$

Substituting $A = \frac{\lambda\alpha Q}{2\pi b\sqrt{K_0\varepsilon}}$ leads to:

$$\Delta p_p = \frac{Q}{2\pi b K_0}\left(\mu_\infty\int_{r_w}^{r_a}\frac{1}{r}dr + (\mu_0-\mu_\infty)\int_{r_w}^{r_a}\frac{1}{1+A^{\chi}r^{-\chi}}\frac{1}{r}dr\right)$$
$$= \frac{Q}{2\pi b K_0}\left(\mu_\infty\int_{r_w}^{r_a}\frac{1}{r}dr + (\mu_0-\mu_\infty)\int_{r_w}^{r_a}\frac{r^{\chi-1}}{r^{\chi}+A^{\chi}}dr\right)$$
$$= \frac{Q}{2\pi b K_0}\left(\mu_\infty\int_{r_w}^{r_a}\frac{1}{r}dr + (\mu_0-\mu_\infty)\frac{1}{\chi}\int_{r_w}^{r_a}\frac{\chi r^{\chi-1}}{r^{\chi}+A^{\chi}}dr\right)$$

After integration, the pressure drop is:

$$\Delta p_p = \frac{Q}{2\pi bK_0}\left(\mu_\infty ln\frac{r_a}{r_w} + \frac{(\mu_0-\mu_\infty)}{\chi}\left(\ln\left(r_a^\chi + A^\chi\right) - \ln\left(r_w^\chi + A^\chi\right)\right)\right) = \frac{Q}{2\pi bK_0}\left(\mu_\infty ln\frac{r_a}{r_w} + \frac{(\mu_0-\mu_\infty)}{\chi}\frac{\ln\left(r_a^\chi + A^\chi\right)}{\ln\left(r_w^\chi + A^\chi\right)}\right)$$

Substituting again $A = \frac{\lambda\alpha Q}{2\pi b\sqrt{K_0\varepsilon}}$ it is possible to get:

$$\Delta p_p = \frac{Q}{2\pi bK_0}\left(\mu_\infty ln\frac{r_a}{r_w} + \frac{(\mu_0-\mu_\infty)}{\chi}\ln\left(\frac{\left(\frac{\lambda\alpha Q}{2\pi b\sqrt{K_0\varepsilon}}\right)^\chi + r_a^\chi}{\left(\frac{\lambda\alpha Q}{2\pi b\sqrt{K_0\varepsilon}}\right)^\chi + r_w^\chi}\right)\right)$$

Appendix B

$$\Delta p_{tot} = \frac{Q}{2\pi bK_0}\left(\mu_\infty ln\frac{r_a}{r_w} + \frac{(\mu_0-\mu_\infty)}{\chi}ln\left(\frac{\left(\frac{\lambda\alpha Q}{2\pi b\sqrt{K_0\varepsilon}}\right)^\chi + r_a^\chi}{\left(\frac{\lambda\alpha Q}{2\pi b\sqrt{K_0\varepsilon}}\right)^\chi + r_w^\chi}\right)\right) + \frac{Q\mu_w}{4\pi bK_0}ln\left(2.25\frac{\rho_w g K_0 t}{\mu_w S_s r_a^2}\right) + \left(\frac{Q}{2\pi b}\right)^2\frac{\beta\rho_w}{r_w}$$

Given that $\mu_\infty = \mu_w + (\mu_\infty - \mu_w)$, we get:

$$\Delta p_{tot} = \frac{Q}{2\pi bK_0}\left(\mu_w ln\frac{r_a}{r_w} + (\mu_\infty-\mu_w)ln\frac{r_a}{r_w} + \frac{(\mu_0-\mu_\infty)}{\chi}\ln\left(\frac{\left(\frac{\lambda\alpha Q}{2\pi b\sqrt{K_0\varepsilon}}\right)^\chi + r_a^\chi}{\left(\frac{\lambda\alpha Q}{2\pi b\sqrt{K_0\varepsilon}}\right)^\chi + r_w^\chi}\right)\right) + \frac{Q\mu_w}{4\pi bK_0}ln\left(2.25\frac{\rho_w g K_0 t}{\mu_w S_s r_a^2}\right) + \left(\frac{Q}{2\pi b}\right)^2\frac{\beta\rho_w}{r_w}$$

Using some algebra:

$$\Delta p_{tot} = \frac{Q\mu_w}{4\pi bK_0}ln\left(2.25\frac{\rho_w g K_0 t}{\mu_w S_s r_a^2}\right) + \frac{Q}{2\pi bK_0}\mu_w ln\frac{r_a}{r_w} + \frac{Q}{2\pi bK_0}\left((\mu_\infty-\mu_w)ln\frac{r_a}{r_w} + \frac{(\mu_0-\mu_\infty)}{\chi}\ln\left(\frac{\left(\frac{\lambda\alpha Q}{2\pi b\sqrt{K_0\varepsilon}}\right)^\chi + r_a^\chi}{\left(\frac{\lambda\alpha Q}{2\pi b\sqrt{K_0\varepsilon}}\right)^\chi + r_w^\chi}\right)\right) + \left(\frac{Q}{2\pi b}\right)^2\frac{\beta\rho_w}{r_w}$$

$$\Delta p_{tot} = \frac{Q\mu_w}{4\pi bK_0}\left(ln\left(\frac{r_a^2}{r_w^2}\cdot 2.25\frac{\rho_w g K_0 t}{\mu_w S_s r_a^2}\right)\right) + \frac{Q}{2\pi bK_0}\left((\mu_\infty-\mu_w)ln\frac{r_a}{r_w} + \frac{(\mu_0-\mu_\infty)}{\chi}\ln\left(\frac{\left(\frac{\lambda\alpha Q}{2\pi b\sqrt{K_0\varepsilon}}\right)^\chi + r_a^\chi}{\left(\frac{\lambda\alpha Q}{2\pi b\sqrt{K_0\varepsilon}}\right)^\chi + r_w^\chi}\right)\right) + \left(\frac{Q}{2\pi b}\right)^2\frac{\beta\rho_w}{r_w}$$

$$\Delta p_{tot} = \frac{Q\mu_w}{4\pi bK_0}\ln 2.25\frac{\rho_w g K_0 t}{\mu_w S_S r_w^2} + \frac{Q}{2\pi bK_0}\left((\mu_\infty-\mu_w)ln\frac{r_a}{r_w} + \frac{(\mu_0-\mu_\infty)}{\chi}\ln\left(\frac{\left(\frac{\lambda\alpha Q}{2\pi b\sqrt{K_0\varepsilon}}\right)^\chi + r_a^\chi}{\left(\frac{\lambda\alpha Q}{2\pi b\sqrt{K_0\varepsilon}}\right)^\chi + r_w^\chi}\right)\right) + \left(\frac{Q}{2\pi b}\right)^2\frac{\beta\rho_w}{r_w}$$

$$\Delta p_{tot} = \frac{Q\mu_w}{4\pi K_0 b}\int_u^\infty \frac{e^{-u}}{u}du + \frac{Q(\mu_\infty-\mu_w)}{2\pi K_0 b}\left(ln\frac{r_a}{r_w} + \left(\frac{\mu_0-\mu_\infty}{\mu_\infty-\mu_w}\right)\frac{1}{\chi}\ln\left(\frac{\left(\frac{\lambda\alpha Q}{2\pi b\sqrt{K_0\varepsilon}}\right)^\chi + r_a^\chi}{\left(\frac{\lambda\alpha Q}{2\pi b\sqrt{K_0\varepsilon}}\right)^\chi + r_w^\chi}\right)\right) + \left(\frac{Q}{2\pi b}\right)^2\frac{\beta\rho_w}{r_w}$$

References

1. Wacławek, S.; Nosek, J.; Cádrová, L.; Antoš, V.; Černík, M. Use of Various Zero Valent Irons for Degradation of Chlorinated Ethenes and Ethanes. *Ecol. Chem. Eng. S* **2015**, *22*, 577–587. [CrossRef]
2. Alazaiza, M.Y.D.; Albahnasawi, A.; Ali, G.A.M.; Bashir, M.J.K.; Copty, N.K.; Amr, S.S.A.; Abushammala, M.F.M.; Al Maska-ri, T. Recent Advances of Nanoremediation Technologies for Soil and Groundwater Remediation: A Review. *Water* **2021**, *13*, 2186. [CrossRef]
3. Mondal, A.; Dubey, B.K.; Arora, M.; Mumford, K. Porous Media Transport of Iron Nanoparticles for Site Remediation Application: A Review of Lab Scale Column Study, Transport Modelling and Field-Scale Application. *J. Hazard. Mater.* **2021**, *403*, 123443. [CrossRef] [PubMed]

4. Němeček, J.; Pokorný, P.; Lacinová, L.; Černík, M.; Masopustová, Z.; Lhotský, O.; Filipová, A.; Cajthaml, T. Combined Abiotic and Biotic In-Situ Reduction of Hexavalent Chromium in Groundwater Using nZVI and Whey: A Remedial Pilot Test. *J. Hazard. Mater.* **2015**, *300*, 670–679. [CrossRef]
5. Czinnerová, M.; Vološčuková, O.; Marková, K.; Ševců, A.; Černík, M.; Nosek, J. Combining Nanoscale Zero-Valent Iron with Electrokinetic Treatment for Remediation of Chlorinated Ethenes and Promoting Biodegradation: A Long-Term Field Study. *Water Res.* **2020**, *175*, 115692. [CrossRef] [PubMed]
6. Mohammadian, S.; Krok, B.; Fritzsche, A.; Bianco, C.; Tosco, T.; Cagigal, E.; Mata, B.; Gonzalez, V.; Diez-Ortiz, M.; Ramos, V.; et al. Field-Scale Demonstration of in Situ Immobilization of Heavy Metals by Injecting Iron Oxide Nanoparticle Adsorption Barriers in Groundwater. *J. Contam. Hydrol.* **2021**, *237*, 103741. [CrossRef]
7. Zhong, L.; Szecsody, J.; Oostrom, M.; Truex, M.; Shen, X.; Li, X. Enhanced Remedial Amendment Delivery to Subsurface Using Shear Thinning Fluid and Aqueous Foam. *J. Hazard. Mater.* **2011**, *191*, 249–257. [CrossRef] [PubMed]
8. Yan, Z.; Ouyang, J.; Wu, B.; Liu, C.; Wang, H.; Wang, A.; Li, Z. Nonmetallic Modified Zero-Valent Iron for Remediating Halogenated Organic Compounds and Heavy Metals: A Comprehensive Review. *Environ. Sci. Ecotechnol.* **2024**, *21*, 100417. [CrossRef]
9. Chen, Z.; Cao, W.; Bai, H.; Zhang, R.; Liu, Y.; Li, Y.; Song, J.; Liu, J.; Ren, G. Review on the Degradation of Chlorinated Hydrocarbons by Persulfate Activated with Zero-Valent Iron-Based Materials. *Water Sci. Technol.* **2023**, *87*, 761–782. [CrossRef] [PubMed]
10. Galdames, A.; Ruiz-Rubio, L.; Orueta, M.; Sánchez-Arzalluz, M.; Vilas-Vilela, J.L. Zero-Valent Iron Nanoparticles for Soil and Groundwater Remediation. *Int. J. Environ. Res. Public Health* **2020**, *17*, 5817. [CrossRef] [PubMed]
11. Wei, J.; Chen, Y.; Dong, Q.; Fan, C.; Zou, M. Dynamic Shear Responses of Combined Contaminated Soil Treated with Nano Zero-Valent Iron (nZVI) under Controlled Moisture. *Sustainability* **2023**, *16*, 289. [CrossRef]
12. Duan, C.; Ren, J.; Tao, L.; Ren, H.; Wang, M.; Wang, B. Study of the Remediation Effect and Mechanism of Biochar-Loaded nZVI on Heavy Metal Contaminated Soil. *Sustainability* **2023**, *15*, 16753. [CrossRef]
13. Antia, D.D.J. Hydrodynamic Decontamination of Groundwater and Soils Using ZVI. *Water* **2023**, *15*, 540. [CrossRef]
14. Gastone, F.; Tosco, T.; Sethi, R. Green Stabilization of Microscale Iron Particles Using Guar Gum: Bulk Rheology, Sedimentation Rate and Enzymatic Degradation. *J. Colloid Interface Sci.* **2014**, *421*, 33–43. [CrossRef]
15. Eljamal, R.; Eljamal, O.; Maamoun, I.; Yilmaz, G.; Sugihara, Y. Enhancing the Characteristics and Reactivity of nZVI: Polymers Effect and Mechanisms. *J. Mol. Liq.* **2020**, *315*, 113714. [CrossRef]
16. Sakulchaicharoen, N.; O'Carroll, D.M.; Herrera, J.E. Enhanced Stability and Dechlorination Activity of Pre-Synthesis Stabi-lized Nanoscale FePd Particles. *J. Contam. Hydrol.* **2010**, *118*, 117–127. [CrossRef]
17. Zhong, L.; Oostrom, M.; Truex, M.J.; Vermeul, V.R.; Szecsody, J.E. Rheological Behavior of Xanthan Gum Solution Related to Shear Thinning Fluid Delivery for Subsurface Remediation. *J. Hazard. Mater.* **2013**, *244–245*, 160–170. [CrossRef]
18. Al-Qenae, A.; Shokri, J.; Shende, T.; Sahimi, M.; Niasar, V. Enhanced Dispersion in Shear-Thinning Fluid Flow through Porous Media. *Phys. Rev. Fluids* **2025**, *10*, 063802. [CrossRef]
19. Cheremisinoff, N.P. *Encyclopedia of Fluid Mechanics*; CRC Press: Boca Raton, FL, USA, 1988; Volume 7.
20. Cross, M.M. Rheology of Non-Newtonian Fluids: A New Flow Equation for Pseudoplastic Systems. *J. Colloid Sci.* **1965**, *20*, 417–437. [CrossRef]
21. Carreau, P.J. Rheological Equations from Molecular Network Theories. *Trans. Soc. Rheol.* **1972**, *16*, 99–127. [CrossRef]
22. Lindner, A.; Bonn, D.; Meunier, J. Viscous Fingering in a Shear-Thinning Fluid. *Phys. Fluids* **2000**, *12*, 256–261. [CrossRef]
23. Darcy, H. *Les Fontaines Publiques de La Ville de Dijon: Exposition et Application. . .*; Victor Dalmont: Paris, France, 1856.
24. Hassanizadeh, S.M.; Gray, W.G. High Velocity Flow in Porous Media. *Transp. Porous Med.* **1987**, *2*, 521–531. [CrossRef]
25. Levy, A.; Levi-Hevroni, D.; Sorek, S.; Ben-Dor, G. Derivation of Forchheimer Terms and Their Verification by Application to Waves Propagation in Porous Media. *Int. J. Multiph. Flow* **1999**, *25*, 683–704. [CrossRef]
26. Dybbs, A.; Edwards, R.V. A New Look at Porous Media Fluid Mechanics—Darcy to Turbulent. In *Fundamentals of Transport Phenomena in Porous Media*; Bear, J., Corapcioglu, M.Y., Eds.; Springer: Dordrecht, The Netherlands, 1984; pp. 199–256, ISBN 978-94-009-6175-3.
27. Forchheimer, P. Wasserbewegung Durch Boden. *Z. Ver. Dtsch. Ing.* **1901**, *45*, 1782–1788.
28. Locatelli, L.; Binning, P.J.; Sanchez-Vila, X.; Søndergaard, G.L.; Rosenberg, L.; Bjerg, P.L. A Simple Contaminant Fate and Transport Modelling Tool for Management and Risk Assessment of Groundwater Pollution from Contaminated Sites. *J. Contam. Hydrol.* **2019**, *221*, 35–49. [CrossRef]
29. Geertsma, J. Estimating the Coefficient of Inertial Resistance in Fluid Flow Through Porous Media. *Soc. Pet. Eng. J.* **1974**, *14*, 445–450. [CrossRef]
30. Moutsopoulos, K.N.; Papaspyros, I.N.E.; Tsihrintzis, V.A. Experimental Investigation of Inertial Flow Processes in Porous Media. *J. Hydrol.* **2009**, *374*, 242–254. [CrossRef]

31. Li, D.; Engler, T.W. Literature Review on Correlations of the Non-Darcy Coefficient. In Proceedings of the SPE Permian Basin Oil and Gas Recovery Conference, Midland, TX, USA, 15–17 May 2001; pp. 106–113.
32. Mathias, S.A.; Moutsopoulos, K.N. Approximate Solutions for Forchheimer Flow during Water Injection and Water Production in an Unconfined Aquifer. *J. Hydrol.* **2016**, *538*, 13–21. [CrossRef]
33. Tosco, T.; Gastone, F.; Sethi, R. Guar Gum Solutions for Improved Delivery of Iron Particles in Porous Media (Part 2): Iron Transport Tests and Modeling in Radial Geometry. *J. Contam. Hydrol.* **2014**, *166*, 34–51. [CrossRef] [PubMed]
34. Bird, R.B.; Lightfoot, E.N.; Stewart, W.E. Transport Phenomena. *AIChE J.* **2002**, *7*, 5J–6J. [CrossRef]
35. Perrin, C.L.; Tardy, P.M.J.; Sorbie, K.S.; Crawshaw, J.C. Experimental and Modeling Study of Newtonian and Non-Newtonian Fluid Flow in Pore Network Micromodels. *J. Colloid Interface Sci.* **2006**, *295*, 542–550. [CrossRef] [PubMed]
36. Sethi, R.; Molfetta, A.D. *Groundwater Engineering: A Technical Approach to Hydrogeology, Contaminant Transport and Groundwater Remediation*; Springer Tracts in Civil Engineering; Springer International Publishing: Berlin/Heidelberg, Germany, 2019; ISBN 978-3-030-20514-0.
37. Thiem, G. *Hydrologische Methoden*; Gebhardt: Streetsboro, OH, USA, 1906.
38. Cooper, H.H.; Jacob, C.E. A Generalized Graphical Method for Evaluating Formation Constants and Summarizing Well-Field History. *Eos Trans. Am. Geophys. Union* **1946**, *27*, 526–534. [CrossRef]
39. Theis, C.V. The Relation between the Lowering of the Piezometric Surface and the Rate and Duration of Discharge of a Well Using Ground-Water Storage. *Eos Trans. Am. Geophys. Union* **1935**, *16*, 519–524. [CrossRef]
40. Bianco, C.; Tosco, T.; Sethi, R. MNMs 2021 Software (Micro- and Nanoparticle Transport, Filtration, and Clogging Model-Suite). Available online: https://www.polito.it/groundwater/software/mnms/ (accessed on 10 October 2024).
41. Mondino, F.; Piscitello, A.; Bianco, C.; Gallo, A.; de Folly D'Auris, A.; Tosco, T.; Tagliabue, M.; Sethi, R. Injection of Zerovalent Iron Gels for Aquifer Nanoremediation: Lab Experiments and Modeling. *Water* **2020**, *12*, 826. [CrossRef]

Disclaimer/Publisher's Note: The statements, opinions and data contained in all publications are solely those of the individual author(s) and contributor(s) and not of MDPI and/or the editor(s). MDPI and/or the editor(s) disclaim responsibility for any injury to people or property resulting from any ideas, methods, instructions or products referred to in the content.